# POLARIMETRIC RADAR AND ELECTRICAL OBSERVATIONS OF DMC ACROSS NORTHERN ALABAMA DURING THE DC3 EXPERIMENT

**4A.5**

Anthony L. Bain[1,] Retha Matthee, and Lawrence D. Carey
UAHuntsville, Severe Weather Institute and Radar & Lightning Laboratories (SWIRLL), Huntsville, AL

## 1. INTRODUCTION

The Deep Convective Clouds and Chemistry Experiment, hereafter, DC3, was an interdisciplinary study that aimed to understand the relationship between kinematic and microphysical properties of deep moist convection (DMC) and resultant lightning characteristics. Detailed documentation of storm kinematics was desirable to better understand the transport of various emissions throughout the depth of the troposphere via DMC and their impact on lightning production. Microphysical information from polarimetric weather radar was utilized during DC3 to identify hydrometeors that are theorized to be relevant for thunderstorm electrification.

Laboratory experiments conducted by Takahashi (1978), Saunders (1994) and Saunders and Peck (1998) as well as numerous observational studies have supported the theory of non-inductive charging (NIC) for cloud electrification. In NIC, stochastic rebounding collisions between rimed graupel/small hail and ice particles in the presence of supercooled water results in the opposite charging of each particle. Gravitational forces, via differences in terminal fallspeed between these hydrometeors, along with convective motions in a vigorous updraft are theorized to result in storm scale charge separation and the generation of an electric field necessary for lightning. Empirical relationships derived by Takahashi (1978) showed that the vertical gradient of the electric field was proportional to both the number and the rate of electrification of rimed graupel/small hail particles. Furthermore, Takahashi (1978) noted that the rate of electrification of rimed graupel/small hail was dependent on the size of the graupel/small hail particle.

The use of radar (both reflectivity and polarimetric radar observations) in numerous observational studies has proven to be a reliable tool for determining hydrometeor type (Carey and Rutledge 1996, 2000; Wiens et al. 2000; Deierling et al. 2008; Woodard et al. 2012). These observational studies have often compared some type of radar observable (e.g. graupel mass, graupel volume) to a lightning property (e.g. total lightning flash rate). Carey and Rutledge (1996); Wiens et al. (2005); Kuhlman et al. (2006) showed that graupel echo volume (using a variety of techniques) often was the best correlation between a radar derived parameter and mean total lightning flash rate. Wiens et al. (2005) used a fuzzy logic hydrometoer identification algorithm to identify graupel particles within supercellular convection during the Severe Thunderstorm Electrification and Precipitation Study (STEPS). Analyzing the supercellular convection that was observed by Wiens et al. (2005), Kuhlman et al. (2006) reported that model simulations revealed strong correlations between model derived total lightning flash rate and graupel volume. Carey and Rutledge (1996) used a combination of polarimetric variables and took a Boolean logic approach to identify graupel for multicellular convection on the Colorado Front Range. Carey and Rutledge (2000) demonstrated that the total flash rate of tropical DMC was well correlated with polarimetric radar inferred precipitation ice mass. Deierling et al. (2008) showed that graupel/small hail mass also trended well with mean total lightning flash rate with storms from the front range of CO as well as storms across northern Alabama. Observations from Deierling and Petersen (2008) and modeling work done by Kuhlman et al. (2006) found that the updraft volume of greater than 5 m $s^{-1}$ was strongly correlated to the mean total lightning flash rate. Interestingly enough, there is some consensus that the updraft volume of greater than 5 m $s^{-1}$ offers superior performance to that of the maximum updraft velocity-lightning flash rate power law relationship used in cloud-resolving models to predict lightning (Price 1992; Barthe et al. 2010). In fact, Barthe et al. 2010 noted in a modeling study that the updraft volume of greater than 5 m $s^{-1}$ was the least reliable predictor of observed total lightning flash rate for two case events.

The specific lightning characteristics that are of interest to the DC3 community include total lightning flash rate, flash density, and flash extent. A modeling study conducted by Barthe et al. (2010) has attempted to estimate total lightning flash rate from a collection of DMC properties (e.g. maximum updraft

1 *Corresponding author address:* Lamont Bain, UAHuntsville
320 Sparkman Drive, Huntsville, AL 3581
Email: Lamont.Bain@nsstc.uah.edu

speed, ice mass flux) using a cloud-resolving model (e.g. Weather & Research Forecasting model). Quantities such as total lightning flash rate and flash extent are used to quantify the production of nitrogen oxides from lightning. Lamarque et al. (1996) and Pickering et al. (1998) showed through the use of global chemical models that nitrogen oxides ($NO_X$) produced via lightning or $LNO_X$ is the largest contributor to the creation of upper tropospheric $NO_X$. $NO_X$ has been thought of as one of the key catalysts for the development of greenhouse gases, particularly ozone ($O_3$) (Pickering et al. 1998; Dye et al. 2000). Based on cases from the Stratospheric-Tropospheric Experiment: Radiation, Aerosols and Ozone (STERAO) field experiment, Dye et al. (2000) concluded that the bulk of $NO_X$ generated is due largely to the higher frequency of intra-cloud (IC) flashes versus that of cloud-to-ground (CG) flashes. In numerical simulations by Pickering et al. (1998), it was reported that CG's produce a larger instantaneous amount of $NO_X$ when compared to IC's due to the larger energetics associated with CG's.

In this study, we seek to explore the aforementioned relationships between radar parameters (graupel/small hail volume, graupel/small hail mass, and updraft volume > 5 m $s^{-1}$) and total lightning flash rate across northern AL and southern TN for a select number of cases during the DC3 field campaign. In order to sample the kinematic, microphysical and electrical elements of DMC across varying regimes, the field phase of DC3 was conducted over three locations across the continental United States; northeastern Colorado, Oklahoma to west Texas and northern Alabama to southern Tennessee. DC3 was a particularly unique experiment in that it attempted to coordinate sampling of DMC with both aircraft and remote sensing based platforms (e.g. radar, radiosondes, lightning mappers). The focus of this manuscript will be on results from the northern AL/southern TN domain, hereafter the AL domain. The AL domain is comprised of three dual-polarization weather radar each at a distinct wavelength for important documentation of microphysical and kinematic properties of DMC , a lightning mapping array (LMA) that allows for 3-D mapping of total lightning and a mobile sounding vehicle for upper air observations. A map of the AL domain and associated instruments is provided in Fig. 1.

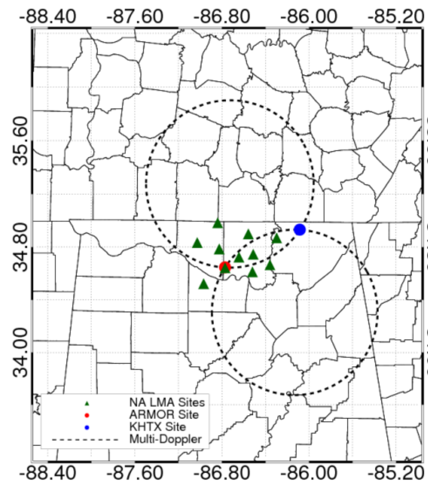


**Figure 1: A map of the DC3 AL domain. The green triangles represent NA LMA VHF antennas. The solid red dot represents the location of the ARMOR radar. The solid blue dot represents the location of KHTX. The short-dashed lines represent regions where multi-Doppler wind synthesis can be performed.**

The S-band, Weather Surveillance Radar – 1988 Doppler (WSR-88D) is operated and owned by the National Weather Service (NWS) and is located at Hytop, AL (KHTX). KHTX is used in this study as well as the C-Band, Advanced Radar for Meteorological and Operational Research radar. ARMOR is located at the Huntsville International Airport (KHSV) and is co-owned by UAHuntsville (UAH) and WHNT. Finally, the Mobile Alabama X-Band radar was deployed to New Market, AL due to the complex terrain and vegetation across the region. This study will only highlight results from KHTX and ARMOR. ARMOR and KHTX have a beamwidth of 1° and .92°, respectively, and both operate in a simultaneous transmit and receive of both the horizontal and vertical channels. ARMOR and KHTX are both capable of measuring horizontal reflectivity ($Z_H$), Doppler velocity ($V_R$), differential reflectivity ($Z_{DR}$), the co-polar correlation coefficient ($\rho_{hv}$) and differential phase ($\Phi_{dp}$). The specific differential phase ($K_{dp}$) for ARMOR is computed using a method that is outlined in Bringi and Chandrasekar (2001). Additional specifications on ARMOR are discussed in Petersen et al. (2005). The relatively close proximity of ARMOR and KHTX (approximately 70 km) presents the opportunity for three dimensional wind retrievals within the highlighted areas denoted in Fig. 1.

Case selections were primarily dictated by the proximity of convection to both the aforementioned multi-Doppler region as well as the proximity to the center of the north AL LMA (NA LMA). NA LMA is operated and owned by the National Aeronautical and Space Administration Marshall Space Flight Center (NASA MSFC) and consists of 11 very high frequency (VHF) antennas across northern AL that detect radiation emissions from propagating leaders associated with lightning (Goodman et al. 2005). Using a time-of-arrival technique highlighted in Cummins et al. (1999), individual points or sources of VHF radiation are detected in space and time and provide a detailed 3-D pictorial view of lightning properties (e.g. flash extent, density). Lightning flashes can be detected reliably at high detection efficiency within about 150 km of the center of the LMA network, thus covering the area within the dual-Doppler lobes. The primary goal of this study is to document convective morphology and resultant electrical properties. Specifically, we seek to explore differences in behavioral trends between microphysical and electrical properties when using particle specific quantities (e.g. precipitation ice mass) versus bulk quantities (e.g. hydrometeor volume) in conjunction with kinematic information obtained from multi-Doppler wind synthesis. With this information, we attempt to develop a useful radar derived quantity-lightning flash rate relationship that can be utilized by atmospheric chemists to parameterize a local Weather Research & Forecasting (WRF) model.

## 2. METHODOLOGY

Both ARMOR and KHTX radar data undergo a vigorous quality control process implemented at the UAH. As a result of ARMOR`s relatively shorter wave length (relative to KHTX), propagation effects occur with the presence of large rain drops and/or melting hailstones. To address this issue, all raw ARMOR data is corrected for attenuation and differential attenuation using a self-consistency method outlined in Bringi et al. (2001). The corrected ARMOR and raw KHTX radar data is then manually inspected using the National Center for Atmospheric Research`s (NCAR) SOLO radar visualization and editing software. During this labor-intensive process, aliased Doppler velocities were corrected and spurious echoes associated with second trip echoes, ground targets and/or anomalous propagation were removed. In the event that ARMOR operations consisted of sector volumes, an internal method for correcting any azimuth pointing angle error was employed. Environmental data from the UAH mobile ballooning facility was quality controlled by specialists at NCAR. For details concerning quality controlled procedures on UAH radiosonde observations (RAOBs), the authors direct the readers to Loehrer et al. (1996). The combination of environmental data and the polarimetric radar information from ARMOR allowed for the use of a fuzzy logic based hydrometeor identification algorithm, hereafter NCAR PID (Vivekanandan et al. 1999; Straka et al. 2000; Deierling et al. 2008). While originally developed for use at S-Band, modifications to the NCAR PID were necessary owing to both ARMOR's wavelength and operational mode (simultaneous transmit of H and V results in the inability to attain the linear depolarization ratio [$L_{DR}$]). With information from NCAR PID, several microphysical quantities thought to be relevant for the non-inductive charging mechanism as outlined in Takahashi (1978), as well as in Saunders (1994), and Saunders and Peck (1998) can be computed. Once the quality control of ARMOR and KHTX data is completed, both sets of data were gridded using NCAR`s REORDER package (Mohr et al. 1986). Polarimetric radar quantities (excluding NCAR PID data) were gridded from radar space to a Cartesian grid with spacing of 1 km in x, y and z using the Cressman Weighting scheme (Cressman 1959) and radii of influence are also 1 km in the horizontal and vertical. The NCAR PID information was also gridded to Cartesian space with 1 km grid spacing in the horizontal and vertical dimensions using a Nearest Neighbor Weighting scheme and similar radii of influence. For this study, graupel/small hail volume and graupel/small hail mass were computed. Consideration was only given to regions between the -10 °C and -40 °C layer. This so-called "charging region", as termed by Latham et al. (2004), is theorized to be the region in which active NIC of rimed graupel/small hail hydrometeors occurs. The number of grid boxes associated with graupel/small hail particles identified by the NCAR PID were summed over the aforementioned layer (layers that corresponded to a given height) and then multiplied by the grid volume to attain the desired graupel/small hail volume. For the estimate of graupel/small hail mass the Rayleigh approximation derived in Carey and Rutledge (2000) for an assumed exponential size distribution was used as seen in Eqn. 1.

$$(1)\ M_{ice} = \Delta x * \Delta y * \Delta z * \pi * \rho_i * N_0^{\frac{3}{7}} * \frac{Z}{720}$$

$$(2)\ Z = \frac{|K|_w^2}{|K|_i^2} * Z_e$$

$$(3)\ M_{ice} = 0.0052 * Z^{0.5}$$

The grid spacing is denoted as Δx, Δy, Δz. The density of ice is denoted as $\rho_i$, $N_O$, is the slope parameter of an assumed exponential size distribution and $Z_e$ is the equivalent radar reflectivity factor following Eqn. 2 from Smith (1984). The density of solid ice (917 kg $m^{-3}$) was assumed for all graupel/small hail particles identified by the NCAR PID. The value of $N_O$ was determined to be 4 x $10^6$ $m^{-4}$, in accordance with typical slope parameter values observed in tropical convection (Petersen 1997). At each grid point in which NCAR PID identified a graupel/small hail particle pixel, Eqns. 1 and 2 were applied within the charging region and summed to arrive at a total graupel/small hail mass (kg). An alternative method to computing graupel/small hail mass is to use a derived radar reflectivity-ice mass ($Z\text{-}M_{ice}$) relationship derived in Heymsfield and Palmer (1986) (Eqn. 3). Sensitivity studies between the Eqns. 1 and 3 did reveal very minor differences between the two methods to compute graupel/small hail mass. The Rayleigh approximation, however, allows for more flexibility with regards to pertinent variables (e.g. slope parameter, ice density, etc.) and was the preferred method for graupel/small hail mass computations herein. After both ARMOR and KHTX radar data are gridded to a common Cartesian plane, NCAR`s Custom Editing and Display of Reduced Cartesian Space (CEDRIC) tool was used for the multi-Doppler wind synthesis (Miller and Frederick 1998). A variational integration method of the mass continuity equation was invoked due to the expected minimization of divergence errors at the upper boundary condition when determining vertical motion from estimates of the U and V components of the horizontal wind as well as estimates of particle fall speed.

As mentioned in the introduction section, NA LMA detects individual VHF radiation emissions or sources. These VHF sources comprise the stepped leader portion of the lightning leader that propagates from some initial point (usually breakdown point) outward into some adjacent charged space. The individual VHF radiation sources were clustered into a lightning flash based on spatial and temporal criteria outlined in McCaul et al. (2005). Furthermore, an additional 10 or more VHF radiation source constraint was applied to the clustered VHF sources in order for it to be classified as a "true" flash in this dataset. This was an attempt to remove erroneous VHF radiation sources (e.g. noise). Sensitivity tests using 5, 10, and 15 VHF radiation source criteria showed very little deviation in terms of the number of flashes between each criteria. Wiens et al. (2005) reported that for higher flash rate events, the selection of a source criterion can have a greater impact on the magnitude of the total lightning flash related calculations, but the total lightning flash trends are conserved. Following Wiens et al. (2005), we decided that a 10 or more source criterion was appropriate for the dataset. In this dataset, there is no upper limit on the amount of VHF radiation sources that can comprise a flash.

As discussed earlier, studies similar to that of Barthe et al. (2010) often sought to relate total lightning flash rate to some radar observable. As a result, this study seeks to develop and test several radar observable-total lightning flash rate relationships. For total lightning flash rate computations, the first VHF radiation source in each flash is stored and counted over a given radar volume (radar volume time is defined as the time between each successive radar volume). The sum of the total lightning flash counts during the radar volume divided by the radar volume time (in minutes) itself yields the total lightning flash rate (# $min^{-1}$).

For all radar and lightning observations, a subjective Lagrangian approach was used to identify and track convective cells (and its associated elements) throughout its lifecycle. Characteristics of the cell or cells of interest (e.g. graupel/small hail volume/mass, initial VHF radiation source) were restricted to a given analysis box drawn subjectively in an attempt to avoid contamination from neighboring convective cells. While tedious, we are confident that this approach is more practical when done subjectively as opposed to an automated cell tracking algorithm for this mode of convection.

The UAH mobile ballooning facility was tasked with taking upper air observations to characterize the environment in which DMC was to develop, but also to support short term forecasting operations. Vertical profiles of temperature, moisture and wind speeds were obtained from the iMet-3150 radiosonde package manufactured by International Met Systems. Pertinent temperature information (e.g. -10 °C level) was obtained from the post-processed NCAR RAOBs.

## 3. RESULTS

### *3.1 DC3 AL Overview*

The results summarized in this paper are for observations of DMC across northern AL. Thus far, five separate convective cell complexes on four different days have been analyzed per Table 1. As was typical across the AL region throughout the entirety of DC3, the regime was characterized as one having very weak deep layer shear, generally less than 20 m $s^{-1}$ and modest positive buoyancy, between 1000 and 1500 J $kg^{-1}$. With weak shear and modest instability, ordinary single to multicellular type convection occurred (Rotunno et al. 1988). The DMC on the 18/19 May 2012 case day is presented to give the reader an idea of a typical environment across DC3 AL.

**Table 1: A summary of select DC3 AL cases for this study.**

| Date | Radars | ARMOR-to-DMC Distance (km) | Mode | Cell Designation |
|---|---|---|---|---|
| 05/18-19/2012 | ARMOR KHTX MAX | 15-20 | Multi-Cell | A1 |
| 05/21/2012 | ARMOR KHTX MAX | 60-65 | Multi-Cell | B1, B2 |
| 06/11/2012 | ARMOR KHTX MAX | 90-95 | Multi-Cell | C1 |
| 06/14/2012 | ARMOR KHTX MAX | 65-70 | Multi-Cell | D1 |

*3.2 18 May 2012 Case (Convective Complex A1) Summary*

The 1801 UTC RAOB (Fig. 2) from near Fayetteville, TN is thought to be fairly representative of the storms that developed (within 40 km of convective initiation). Values of surface based Convective Available Potential Energy (CAPE) were just below 1000 J $kg^{-1}$ with 0-6 km bulk shear values near 2 m $s^{-1}$ as suggested by visual inspection of vertical profiles of temperature, moisture and wind speeds. Of important note is the Miller type IV (inverted-V), which is typical when afternoon mixing of the boundary layer results in a near dry adiabatic dry-bulb temperature and near constant mixing ratio on the Skew-T log P diagram. This inverted-V type sounding on this afternoon resulted in fair amount of downdraft CAPE (DCAPE) which supported strong thunderstorm downdrafts and subsequent convective outflow. On this case day, the strong convective outflow (and resultant collisions) was the culprit for the genesis of the DMC that is analyzed hereafter. It is important to note that the -10 °C level corresponded to a height around 5 km above ground level (AGL) with the -40 °C being just above 9 km AGL.

*3.3 Convective Initiation and Initial Stages of Convection (2203 UTC)*

Convective initiation of storm complex A1 occurred just after 2200 UTC approximately 18 km north of ARMOR along outflow from convection that developed across northern AL and southern TN. Aloft (at 5 km), storm complex A1 exhibited a broad and weak updraft, based on estimates of vertical velocities (between 2-5 m $s^{-1}$) as observed in Fig. 3. Fig. 4 is a CAPPI at 9 km that reveals that during the early stages of convection, the cumulonimbi showed signs of some vertical depth (30 dBZ at 9 km) but lacked a large and broad updraft. No lightning was observed during the first 15 minutes of A1's lifetime. The absence of any appreciable graupel mass or volume identified from the NCAR PID (e.g., inferred from Fig. 5) suggests that warm rain coalescence processes was the primary microphysical process occurring. This warm rain coalescence process is theorized to be linked to the lack of significant electrification (e.g., Carey and Rutledge 2000). As mentioned earlier, the lack of a robust updraft precluded any lofting of larger supercooled raindrops, which upon freezing allow for graupel/small hail growth in the mixed phase region and thus charging and subsequent cloud electrification in storms with warm cloud bases.

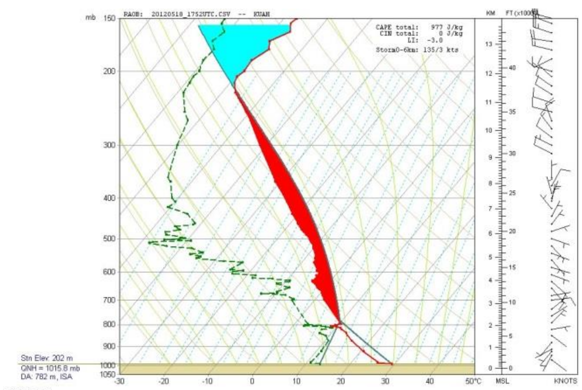

**Figure 2: 1801 UTC RAOB from UAH Mobile Ballooning Facility on 18 May 2012. Balloon was launched from 35.14 °N -86.57 °W.**

*3.4 Initial Cloud Electrification (2215 UTC)*

Initial cloud electrification occurred roughly 15 minutes after 2200 UTC. During this portion of A1's lifecycle, a modest increase in the graupel/small hail volume and mass (Figs. 5 and 6, respectively) occurred. This is likely in response to an increase in the size of the updraft volume > 5 m $s^{-1}$ as seen in Fig. 7. Nearly instantaneous with cloud electrification is the appearance of the $Z_{DR}$ column signature. From

Fig. 8, two separate $Z_{DR}$ columns associated with two separate convective updrafts are discernible within the larger convective complex, A1. With large $Z_{DR}$ values (2 dB) and moderate $Z_H$ (50-55 dBZ) it is likely that oblate millimeter sized liquid particles are being injected upward through the mixed phase region via the two updrafts within A1. ARMOR PPI at 2215 UTC (**Fig. 9**) revealed a slight depression in $\rho_{hv}$ aloft at 4.8 km within A1 located around 15 km north of ARMOR. This depression in $\rho_{hv}$ aloft suggests diversity of hydrometeors. Given the environmental data discussed in section 3.2 a mixture of supercooled rain, partially frozen drops, and/or graupel/hail is likely being sampled by ARMOR. Moreover, the appearance of this freezing signature is consistent with an increase in graupel/small hail volume (fig. 5) and graupel/small hail mass (fig. 6) around 2215 UTC. Estimates of vertical motion throughout the depth of A1's charging zone (roughly 5 to 9 km) do suggest that updraft velocities were in excess of 5 m $s^{-1}$. The updrafts that were sampled during the 2215 UTC timeframe appeared stronger and exhibited a larger degree of vertical continuity (as opposed to the updrafts sampled around 2203 UTC).

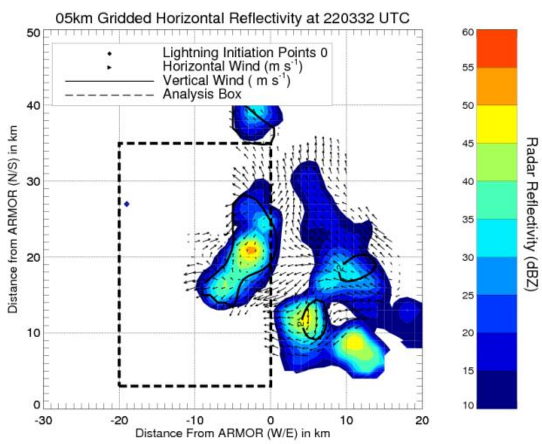


**Figure 3: 05km gridded CAPPI of horizontal reflectivity ($Z_H$, dBZ, shaded as shown), horizontal winds (vectors) and vertical velocities (solid contours, every 5 m $s^{-1}$ starting at 5 m $s^{-1}$) at 220332 UTC from ARMOR radar. The analysis box is shown (dashed line) and bounds cell complex A1.**

### *3.5 Mature Stage (2248 UTC)*

Roughly 20 minutes after the appearance of the $Z_{DR}$ columns a very broad updraft develops at 5 km as seen in Fig. 10. The thunderstorm becomes relatively highly electrified with just over 80 flashes over a 4-5 minute time frame. A strong and broad updraft developed during this time frame in Fig. 10 and maximum vertical velocities around 15-20 m $s^{-1}$ are suggested from multi-Doppler wind synthesis. Most initiation sources in Fig. 10 are clustered around and just outside of the regions of maximum vertical motion. Convective complex A1 approached its peak in terms of lightning activity during the 2248 UTC ARMOR volume with lightning flash rates around 20 flashes $min^{-1}$. During this time, the graupel/small hail volume and mass also peak similar to that of the total lightning flash rate per figs. 5 and 6, respectively.

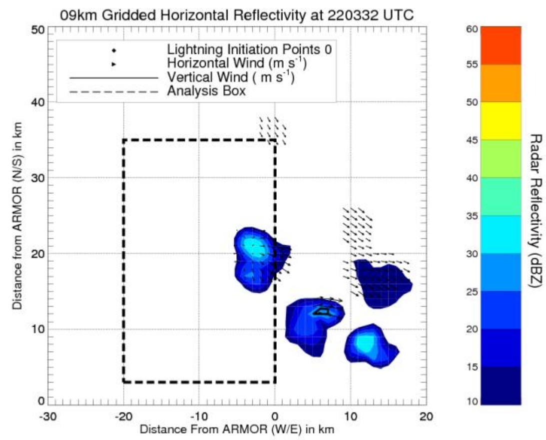


**Figure 4: Same as Fig 3 except for at 09km.**

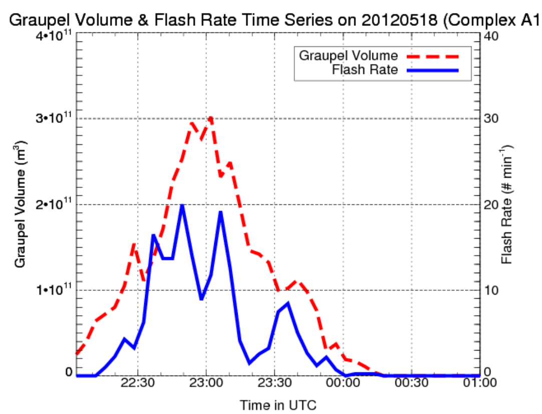


**Figure 5: Time series of graupel/small hail volume and total lightning flash rate for 18 May 2012 DC3 AL case. The dashed red line represents the graupel/small volume ($m^3$) and the solid blue line represents the total lightning flash rate (# $min^{-1}$) per NA LMA.**

### *3.6 Decay Stage (2358 UTC)*

An extensive "orphaned-anvil" developed aloft at 10 km, (Fig. 11) signifying the end of convective complex A1. A decrease in, graupel/small hail volume and mass as well as the updraft volume >

5 m s$^{-1}$ all decrease towards zero with the similar trend in the total lightning flash rate. Time series (Figs. 5-8) clearly illustrate the rapid decrease in all three radar observables with total lightning flash rate. It is during this time that the convective complex A1 is at the end of its lifecycle.

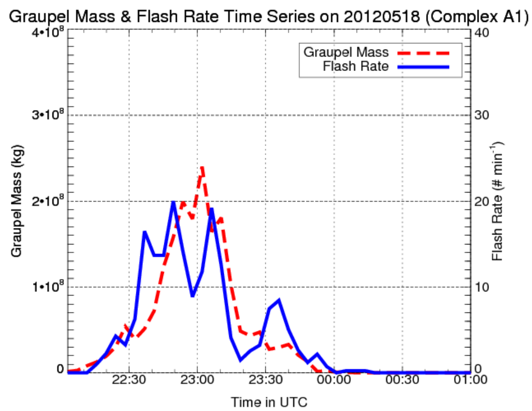


**Figure 6: Time series of graupel/small hail mass and total lightning flash rate for 18 May 2012 DC3 AL case. The dashed red line represents the graupel/small hail mass (kg) and the solid blue line represents the total lightning flash rate (# min$^{-1}$) per NA LMA.**

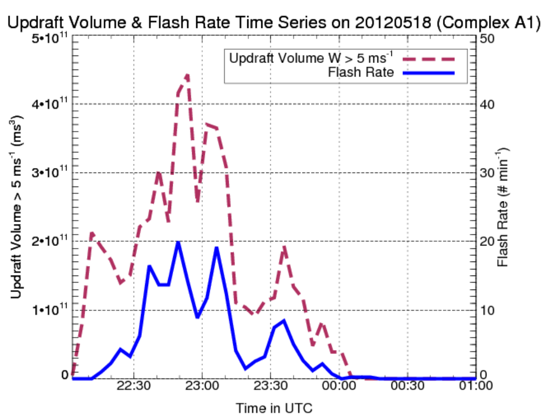


**Figure 7: Time series of updraft volume > 5 m s$^{-1}$ volume and total lightning flash rate for 18 May 2012 DC3 AL case. The dashed faded red line represents the updraft volume > 5 m s$^{-1}$ (m$^3$) and the solid blue line represents the total lightning flash rate (# min$^{-1}$) per NA LMA.**

## 4. DISCUSSION

As noted earlier, the aim of this study is to develop a useful radar observable-total lightning flash rate relationship that can be used in cloud-resolving numerical weather models for the parameterization of flash rates and ultimately the estimation of $LNO_X$. The radar parameters that have been discussed thus far are the graupel/small hail volume, graupel/small hail mass, and the updraft volume of > 5 m s$^{-1}$. To test how well the radar observables and total lightning flash rate correlate, we make use of the Pearson product-moment correlation. In addition, a simple linear least squares regression technique is applied to the entire flash rate vs. radar observable data from DC3 AL in order to derive flash rate parameterizations for the region. The graupel/small hail volume and graupel/small hail mass both have a sample size of 200 while the updraft volume > 5 m s$^{-1}$ has only 136.

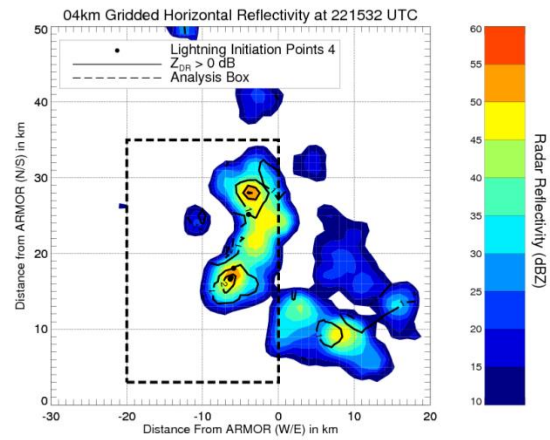


**Figure 8: 04km gridded CAPPI with $Z_H$ (dBZ) in the color filled plot. The solid black contour represents $Z_{DR}$ (dB) beginning at 0 dB with increments of 1 dB. The black diamonds represent NA LMA flash initiation points.**

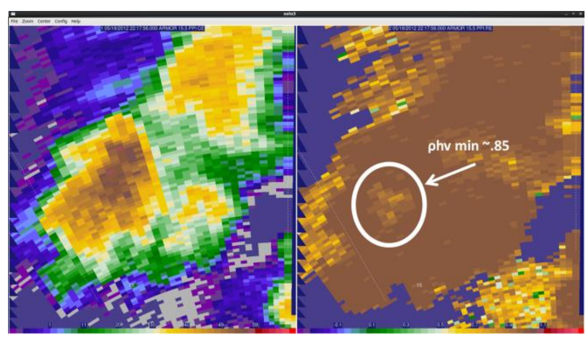


**Figure 9: Plane Position Indicator (PPI) at 15.1° from 2217 UTC elevation angle from ARMOR. The image in the left panel represents $Z_H$ (dBZ) and the image in the right panel represents $\rho_{hv}$.**

The decrease in the sample size for the kinematic quantity is a result of an inability to retrieve accurate estimates of vertical motion during the June 14, 2012 case day. A summary of the Pearson product-moment correlations with their respective ranks, as well as measures of error for the best fit lines developed can be found in Table 2. The best fit lines are given as

Eqns. 4-6. From Table 2, it is apparent that GSHV correlates the best overall across the data set for DC3 AL. This is consistent with previous observational and modeling studies performed by Carey and Rutledge (1996), Wiens et al. (2005) and Kuhlman et al. (2006). From a standpoint of examining the NIC mechanism explicitly, it is perhaps intuitive that the graupel/small hail volume could serve as a proxy for the number of graupel/small hail particles as seen in NIC equations derived by Takahashi (1978).

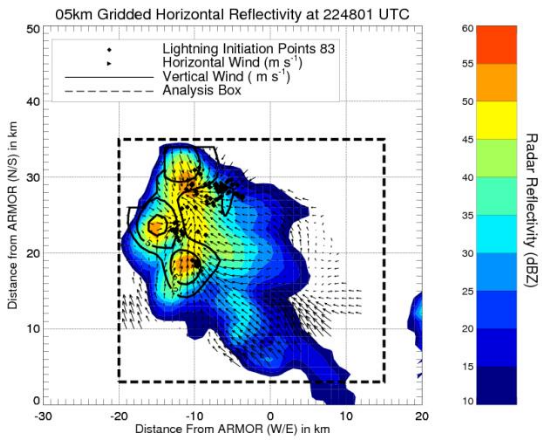


**Figure 10: Same as fig 3, except for at 05km and at 224801 UTC.**

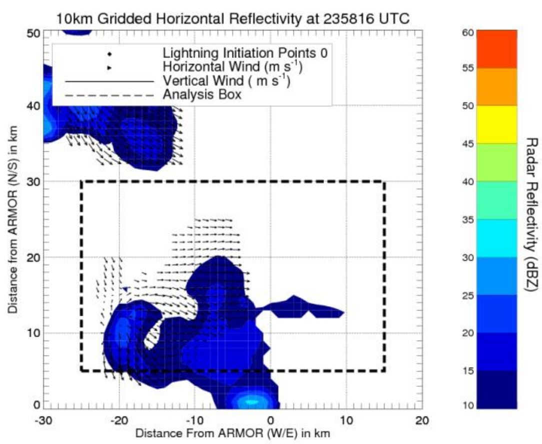


**Figure 11: Same as Fig. 3 except at 10km CAPPI and at 235816 UTC.**

To underscore the importance of graupel/small hail, Williams et al. (2001) and Deierling et al. (2008) note that presence of graupel/small hail is necessary for NIC. Williams et al. (2001) hypothesized that the integrated surface area of hail particles (all hail particles within a convective cell) was smaller than that of graupel. As a result, the amount of charge generated via the NIC for large hail would likely prove to be insufficient. Similar to Deierling et al. (2008), sensitivity tests conducted on the DC3 AL dataset when examining NCAR PID diagnosed graupel/small hail in isolation versus NCAR PID diagnosed graupel/small hail and large hail (relative to other graupel/small hail PID category) mass and volume exhibited very little difference from a correlation standpoint with total lightning. Moreover, the explicitly NCAR PID diagnosed large hail versus total lightning flash rate revealed a poorer correlation. This is consistent with Williams et al. (2001) and Deierling et al. (2008).

**Table 2: Pearson Correlation, Mean Square and Root Mean Square Error with associated ranks.**

| Quantity | Pearson Correlation (Rank) | Mean Square Error (Rank) | Root Mean Square Error (Rank) |
|---|---|---|---|
| Lightning Flash Rate-Graupel/Small Hail Volume | 0.91 (1) | 7.29 (1) | 2.7 (1) |
| Lightning Flash Rate-Graupel/small Hail Mass | 0.85 (2) | 14.73 (3) | 3.57 (3) |
| Lightning Flash Rate- Updraft Volume | 0.65 (3) | 8.13 (2) | 2.8 (2) |

(4) $F = 5.6 \times 10^{-11} \times \mathrm{GSHV}$; n = 200

(5) $F = 1.49 + 6.75 \times 10^{8} \times \mathrm{GSHM}; \ n = 200$

(6) $F = 1.72 \times 10^{-11} \times W_5$ ; n= 136

Both the mean square error (MSE) and root mean square error (RMSE) of the GSHV are smaller than that of the GSHM given in Table 2. While both parameters are likely suitable indicators of total lightning flash rate in a cloud resolving numerical model, the results here would suggest that the GSHV would serve as the best indicator of total lightning flash rate. Finally, the updraft volume showed the least amount of correlation with total lightning flash. Physically, this result is due to the rigid threshold $W_5$ that is invoked over a given convective complex. For very weak convection such as a few case days during DC3 AL and during an event day from Barthe et al. (2010) which took place across northern AL, it is very difficult for sustained vertical motions of $\geq$ 5 m $s^{-1}$ especially in weaker, low total lightning flash rate convective cells and their associated environments. While not explicitly shown, it was found that there was some variability between the $W_5$ in the mixed phase region and total lightning flash rate during DC3 on certain convective cells on various days across DC3 AL. It is probable that weaker convective cells are capable of producing lightning with updraft velocities below 5 m $s^{-1}$. With that notion, we would argue that for weaker convective cells or cell complex, a better kinematic based radar-total lightning flash rate relationship may be attainable if the constraint on the minimum velocity of the updraft volume is relaxed (e.g. > 3 m $s^{-1}$ volume) or the maximum vertical velocity of the convective cell or complex is used. Preliminary tests (not shown) are consistent with that suggestion.

## 5. SUMMARY

We have presented an overview of the environmental, radar and electrical characteristics observed for a multicellular convective complex over northern Alabama on 18 May 2012 during DC3. The entire life cycle of convective complex A1 was examined from a radar and lightning mapper standpoint. The GSHV, GSHM and $W_5$ were examined and linear regression methods revealed that all three correlated with the total lightning flash rate primarily due to the updraft and graupel/small hail's role in the NIC charging processes as outlined by Takahashi (1978), Saunders (1994), Saunders and Peck (1998) and others. Table 2 revealed that GSHV and GSHM were correlated the best with the total lightning flash rate, respectively. It was apparent that $W_5$, however, did not trend well with the total lightning flash rate. While somewhat speculative, it may be plausible that the vertical velocity within weaker convection falls below 5 m $s^{-1}$, while convection is still electrified. As a result $W_5$ de-correlates and becomes a less useful tool. A smaller threshold for weaker convection may be appropriate if the use of a kinematic parameter is desired. Graupel/small hail volume consistently outperformed the other proposed parameters as it possessed the highest correlation with and smallest RMSE in estimating the total lightning flash rate. As a result, the empirical relationship developed here for GSHV could prove to be useful when parameterizing a cloud-resolving numerical model for lightning flash rate and resultant $LNO_X$ computations.

## 6. ACKNOWLEDGEMENTS

We would like to acknowledge Dr. Bradley Smull of the National Science Foundation`s Physical and Dynamical Meteorology Program (AGS-1063573) for whose funding made this research possible. Special thanks also go to Ms. Mariana Felix of UAHuntsville for excellent radar data collection throughout DC3 AL. Finally and certainly not least, special thanks to Elise and Chris Schultz of UAHuntsville for processing of both ARMOR radar data as well as the NA LMA data.

## 7. REFERENCES

Barthe, C., W. Deierling, M.C. Barth, 2010: Estimation of total lightning from various storm parameters: A cloud-resolving model study. *J. Geophys Res.,* **115**, D24202

Bringi, V.N., T.D. Keenan, V., Chandrasekar, 2001: Correcting C-Band radar Reflectivity and Differential Reflectivity Data for Rain Attenuation: A Self-Consistent Method With Constraints. *IEEE Transc on Geo. And Rem. Sens*, **39**, 1906-1915

Carey, L. D., S.A. Rutledge, 1996: A multiparameter radar case study of the microphysical and kinematic evolution of a lightning producing storm, *J. Meteorol. Atmos. Phys*., **59**, 33–64.

Carey, L. D., S.A. Rutledge, 2000, The Relationship between Precipitation and Lightning in Tropical Island Convection: A C-Band Polarimetric Radar Study. *Mon. Wea. Rev.*, **128**, 2687–2710.

Cressman G.P., 1959: An Operational Objective Analysis System. *Mon. Wea. Rev.,* **87**, 367-374

Cummins K. L., R.B. Pyle, G. Fournier, 1999: AN integrated North American Lightning Detection Network. *Proc. 11th Int. Conf. on Atmospheric Electricity,* Guntersville, AL, ICAE, 218-221

Deierling, W., W.A. Petersen , J. Lantham, S. Ellis., H.J. Christian Jr., 2008: The relationship between lightning activity and ice fluxes in thunderstorms, *J. Geophys Res*., **113**, D15210

______, W.A. Petersen, 2008: Total lightning activity as an indicator of updraft characteristics. *J. Geophys Res.,* **113,** D16210

Dye J.E., B.A. Ridley, W. Skamarock, M. Barth, M. Venticinque, E. Defer, P. Blanchet, C. Thery, P. Laroche, K. Baumann, G. Hubler, DD. Parrish, T. Ryerson, M. Trainer, G. Frost, J.S. Holloway, T. Matejka, D. Bartels, F.C. Fehsenfeld, A. Tuck, S.A. Rutledge, T. Lang, J.Stith, R. Zerr, 2000: An overview of the Stratospheric-Tropospheric Experiment Radiation, Aerosols, and ozone (STERAO)-Deep

Convective experiment with results for the July 10, 1996 storm. *J. Geophys. Res.,* **105**, D810023

Goodman S.J, R. Blakeslee, H. Christian, W. Koshak, J. Bailey, J. Hall, E. McCaul, D. Buechler, C. Darden, J. Burks, T. Bradshaw, P. Gatlin, 2005: The North Alabama Lightning Mapping Array: Recent severe storm observations and future prospects. *Atmos. Res.,* **76,** 423-437

Heymsfield, A. J., and A. G. Palmer (1986), Relations for deriving thunderstorm anvil mass of CCOPE storm water budget estimates, *J. Clim. Appl. Meteorol.,* **25**, 691– 702

Kuhlman K.M., C. I., Ziegler, E.R. Mansell, D.R. MacGorman, J.M. Straka., 2006: Numerically Simulated Electrification and Lightning of the 29 June 2000 STEPS Supercell Storm. *Mon. Weather. Rev.* **134**, 2734-2757.

Lamarque, J.-F., G. Brasseur, P. Hess, J.-F. Müller, 1996: Three-dimensional study of the relative contributions of the different nitrogen sources in the troposphere. *J. Geophys. Res.,* **22**, 955-22,968,

Latham, J., A. M. Blyth, H. J. Christian Jr., W. Deierling, and A. M. Gadian., 2004: Determination of precipitation rates and yields from lightning measurements, *J. Hydrol*., **288** (1–2), 13– 19.

Loehrer, S.M., T.A. Edmands, and J.A. Moore, 1996: TOGA COARE Upper-Air Sounding Data Archive: Development and quality control procedures. *Bull. Amer. Meteor. Soc.*, **77**, 2651-2672

McCaul Jr., E.W., J.C. Bailey, J. Hall, S.J. Goodman, R.J. Blakeslee, and D.E. Buechler., 2005: A Flash Clustering Algorithm for North Alabama Lightning Mapping Array data, *Conf. on Meteor. App. Of Lightning Data Preprints.,* San Diego, CA

Mohr, C.G., L.J. Miller, R.L. Vaughn, and H.W. Frank 1986: On the merger of mesoscale datasets into a common Cartesian format for efficient and systematic analysis, *J. Atmos Oceanic. Technol.,* **3**, 143-161.

Miller, L. Jay and T. Frederick 1998: Earth Observation Laboratory's Radar Data Analysis Tools, https://wiki.ucar.edu/display/raygridding/home

Pickering, K. E., Y. Wang, W.-K. Tao, C. Price, and J.-F. Mueller, 1998: Vertical distributions of lightning NOx for use in regional and global chemical transport models, *J. Geophys. Res.,* 103, D231203

Petersen, W. A., 1997: Multi-scale process studies in the tropics: Results from lightning observations. Ph.D. dissertation, Colorado State University, 354 pp.

Price, C., D. Rind, 1996: A simple lightning parameterization for calculating global lightning distributions. *J. Geophys, Res.,* **97**, 9919-9933

Pruppacher, H.R., and J.D. Klett, 1997: Microphysics and Clouds and Precipitations, Kluwer Acad., Dordrecht, Netherlands.

Rotunno, R., J.B. Klemp, and M.L. Weisman, 1988: A theory for strong, long-lived squall lines. *J. Atmos. Sci.,* **45**, 463-485.

Saunders, C.P.,R., 1994: Thunderstorm electrification laboratory experiments and charging mechanisms. *J. Geophys. Res.,* **99**, 10773-10779

_________, and S. L. Peck 1998: Laboratory studies of the influence of the rime accretion rate on charge transfer during crystal/graupel collisions, J. Geophys.Res., 103(D12),13949–13956, doi:10.1029/97JD02644.

Smith, P. L., 1984: Equivalent Radar Reflectivity Factors for Snow and Ice Particles. *J. Climate Appl. Meteor.*, **23**, 1258–1260.

Straka, J. M., D. S. Zrnić, R.V. Ryzhkov, 2000: Bulk Hydrometeor Classification and Quantification Using Polarimetric Radar Data: Synthesis of Relations. *J. Appl. Meteor.*, **39**, 1341–1372.

Takahashi, T., 1978: Riming electrification as a charge generation mechanism in thunderstorms. *J. Atmos. Sci.,* **35,** 1536-1548.

Vivekanandan, J., D.S. Zrnic, S. Ellis, R. Oye, and A.V. Ryzhkov, 1999: Cloud Microphysics Retrievals Using S-Band Dual-Polarization Radar Measurements. *BAMS*., **80**, 381-388.

Wiens, K. C., S.A. Rutledge, S.A., Tessendorf, 2005: The 29 June 2000 Supercell observed during STEPS. Part II: Lightning and Charge Structure. *J. Atmos. Sci.,* **62**, 4151-4177.

Williams E.R., 2001: The electrification of severe storms. *Severe Convective Storms, Meteor. Monogr.,* No. 50, Amer. Meteor. Soc., 527-561

Woodard, C.J., L. D. Carey, W.A., Petersen, W.P., Roeder, 2012: Operational utility of dual-polarization variables in lightning initiation forecasting. *Electronic J. Operational Meteor.,* **13**, 79-102.